STRUCTURAL CHEMISTRY

ISSN: 2053-2296
journals.iucr.org/c

Nontypical iodine–halogen bonds in the crystal structure of (3*E*)-8-chloro-3-iodomethylidene-2,3-dihydro-1,4-oxazino[2,3,4-*ij*]quinolin-4-ium triiodide

E. V. Bartashevich, V. I. Batalov, I. D. Yushina, A. I. Stash and Y. S. Chen

Acta Cryst. (2016). C**72**, 341–345

Acta Cryst C STRUCTURAL CHEMISTRY
ISSN 2053-2296

Nontypical iodine–halogen bonds in the crystal structure of (3*E*)-8-chloro-3-iodomethylidene-2,3-dihydro-1,4-oxazino[2,3,4-*ij*]quinolin-4-ium triiodide

E. V. Bartashevich,[a]* V. I. Batalov,[a] I. D. Yushina,[a] A. I. Stash[b] and Y. S. Chen[c]

[a]Faculty of Chemistry, South Ural State University, Lenin Prospect 76, Chelyabinsk 454080, Russian Federation, [b]Laboratory of Oxide Materials, Karpov Institute of Physical Chemistry, Vorontsovo Pole St. 10, Moscow 105064, Russian Federation, and [c]The University of Chicago, 5801 S Ellis Ave, Chicago, Illinois 60637, USA. *Correspondence e-mail: kbartash@yandex.ru

Received 15 February 2016
Accepted 8 March 2016

Edited by V. Langer, Chalmers University of Technology, Sweden

Keywords: halogen bond; dihydro-oxazinoquinolinium triiodide; triiodide–triiodide interactions; Raman spectra; thermal analysis; crystal structure; synchrotron study.

CCDC reference: 1459305

Supporting information: this article has supporting information at journals.iucr.org/c

Two kinds of iodine–iodine halogen bonds are the focus of our attention in the crystal structure of the title salt, $C_{12}H_8ClINO^+\cdot I_3^-$, described by X-ray diffraction. The first kind is a halogen bond, reinforced by charges, between the I atom of the heterocyclic cation and the triiodide anion. The second kind is the rare case of a halogen bond between the terminal atoms of neighbouring triiodide anions. The influence of relatively weakly bound iodine inside an asymmetric triiodide anion on the thermal and Raman spectroscopic properties has been demonstrated.

1. Introduction

Halogen bonds fulfill a major function in the crystal structure formation of a wide range of halogenated organic compounds (Metrangolo *et al.*, 2008; Gilday *et al.*, 2015). Halogen bonding is defined as the electrostatic attraction between a nucleophilic region of any atom and the region with increased electrostatic potential that is formed on a halogen atom in the direction of the extension of its covalent bond with another atom (Desiraju *et al.*, 2013). Heterocyclic cations containing covalently bonded iodine have demonstrated a predisposition to halogen bonding with oligo- or polyiodide anions in crystals (Bartashevich *et al.*, 2014). Such iodine-saturated compounds composed of an organic cation and a polyiodide anion with iodine storage features can be used as iodophors for water disinfection (Punyani *et al.*, 2006). The practical importance of compounds with iodine–iodine halogen bonds makes it of interest to study the nature of such interactions in crystals. Hence, identification of the factors that are responsible for the strength of iodine retention in crystals seems relevant. Iodine-containing heterocyclic cations are usually formed during the iodocyclization of alkenylthio(oxy)quinoline esters (Kim, 2008). We have noted earlier (Bartashevich *et al.*, 2015) that the presence of a Csp^2—I fragment in the organic part inevitably leads to 'reinforced-by-charges' halogen bonding between a heterocyclic cation and an oligoiodide anion. If the counter-ions are triiodide ions, then the electron-donor atoms are the terminal atoms of the triiodide anions.

The halogen–halogen noncovalent interactions are the focus of our attention in the crystal structure of the title salt, (3*E*)-8-chloro-3-iodomethylidene-2,3-dihydro-1,4-oxazino-[2,3,4-*ij*]quinolin-4-ium triiodide, (1). The following dilemma was of primary interest: the halogen-substituted heterocyclic

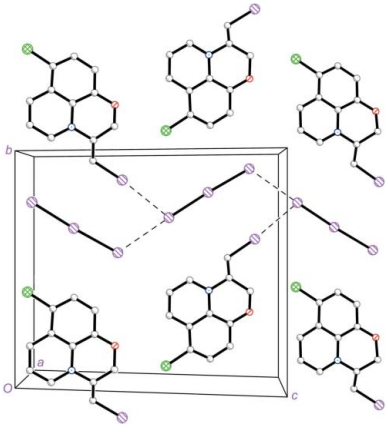

Table 1
Experimental details.

Crystal data	
Chemical formula	$C_{12}H_8ClINO^+\cdot I_3^-$
M_r	725.24
Crystal system, space group	Monoclinic, $P2_1/n$
Temperature (K)	100
a, b, c (Å)	7.6227 (2), 13.9464 (4), 16.0161 (4)
β (°)	101.6439 (7)
V (Å^3)	1667.62 (8)
Z	4
Radiation type	Synchrotron, λ = 0.41328 Å
μ (mm^{-1})	1.75
Crystal size (mm)	0.04 × 0.03 × 0.01
Data collection	
Diffractometer	Bruker APEXII CCD
Absorption correction	Multi-scan (*SADABS*; Bruker, 2013)
T_{min}, T_{max}	0.842, 0.955
No. of measured, independent and observed [$I > 2\sigma(I)$] reflections	45635, 5066, 4500
R_{int}	0.048
(sin $\theta/\lambda)_{max}$ (Å^{-1})	0.714
Refinement	
$R[F^2 > 2\sigma(F^2)]$, $wR(F^2)$, S	0.016, 0.035, 1.04
No. of reflections	5066
No. of parameters	172
H-atom treatment	H-atom parameters constrained
$\Delta\rho_{max}$, $\Delta\rho_{min}$ (e Å^{-3})	0.59, −0.52

Computer programs: *APEX2* (Bruker, 2013), *SAINT* (Bruker, 2013), *SHELXS97* (Sheldrick, 2008), *SHELXL2013* (Sheldrick, 2015), *SHELXTL* (Bruker, 2013), *ACD/ChemSketch* (Advanced Chemistry Development Inc., 2015) and *SHELXTL* (Bruker, 2013).

cation includes both I and Cl atoms, but only iodine participates as an acceptor of electrons in halogen bonding with the triiodide anion. The secondary question was the unusual halogen bond between different terminal atoms of neighbouring triiodide anions, *i.e.* $I_3^-\cdots I_3^-$. We observed the rare case of a Type II noncovalent interaction (Metrangolo & Resnati, 2014) generated by similarly charged ions. Therefore, we decided to use Raman spectroscopy and thermal analysis techniques in order to study how noncovalent interactions influence the physical properties of the studied salt.

2. Experimental

2.1. Synthesis and crystallization

The title compound was synthesized in two steps from 5-chloroquinolin-8-ol (Sigma–Aldrich). The first step was the routine alkylation of an aromatic phenol. Annealed potassium carbonate (0.690 g, 5 mmol) was added to a solution of 5-chloroquinolin-8-ol (0.449 g, 2.5 mmol) in acetone (20 ml) placed in a round-bottomed flask. The mixture was heated to 323 K with stirring and a solution of allyl bromide (3.18 mmol, 1.25 equivalents) in toluene (0.35 ml, 80%) was added. The resulting mixture was kept at 323 K for 20 h with stirring. The precipitate was filtered off and washed with acetone. The filtrate was evaporated *in vacuo* and the residue was dissolved in dichloromethane and dried with anhydrous magnesium sulfate. The resulting solution was decanted and the solvent was evaporated *in vacuo*, giving a brown powder of 5-chloro-8-(prop-2-yn-1-yloxy)quinoline (see Scheme) (yield 0.478 g, 56%).

The second step was the reaction of 5-chloro-8-(prop-2-yn-1-yloxy)quinoline with iodine, giving the heterocyclization product. 5-Chloro-8-(prop-2-yn-1-yloxy)quinoline (0.055 g, 0.25 mmol) was dissolved in dichloromethane (5 ml) and mixed with a solution of iodine (0.191 g, 0.75 mmol) in dichloromethane (5 ml). The resulting mixture was kept in a closed flask at room temperature for 12 h and brown crystals of the final product were collected. The solution was decanted, giving salt (1) (yield 0.174 g, 96%).

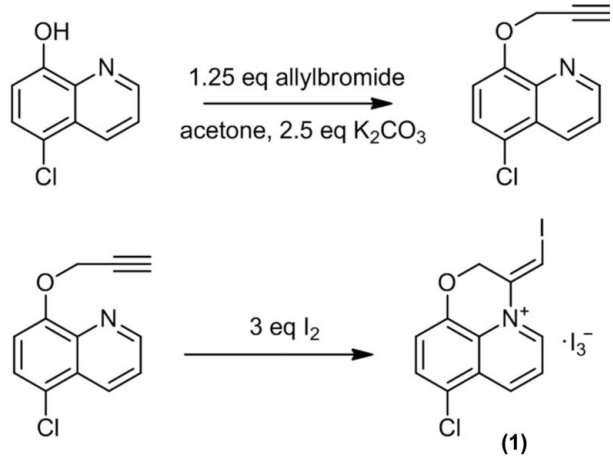

2.2. Data collection and refinement

The diffraction study was performed using synchrotron radiation at the ChemMatCARS beam line (ID-15) at the Advanced Photon Source, Argonne National Laboratory (Argonne, IL). The data collection was carried out using a wavelength of 0.41328 Å obtained from a diamond (111) monochromator. The minimum exposure time of 0.3 s was not enough to obtain all strong reflections without saturating the CCD detector based on a Bruker 6000 and this led to the loss of seven strong reflections.

Crystal data, data collection and structure refinement details are summarized in Table 1. The coordinates of the H atoms were calculated and refined using a riding model, with C—H = 0.99 Å for methylene H atoms and C—H = 0.95 Å otherwise, and with U_{iso}(H) = 1.2U_{eq}(C).

2.3. Thermal analysis and spectroscopic experiment

Thermal analysis data were recorded over the temperature range 298–970 K using Netzsch STA F1 equipment at a heating rate of 10 K min^{-1} in corundum crucibles in air.

Raman spectra were recorded on a Triplemate SPEX spectrometer with a CCD detector (LN-1340PB) from Princeton Instruments. The 632.8 nm line of an He–Ne$^+$ laser was used for spectral excitation. The samples were placed in the focal plane of a Zeiss LD Epiplan 40X/0.60 Pol objective with a 2 mm working distance and an aperture of 0.6, which was used for laser beam focusing and the collection of scattered light. The diameter of the laser beam on the sample surface

was 2 µm. The spectra were measured in a 180° backscattering collection geometry with a Raman microscope. All measurements were performed with a spectral resolution of 2.0 cm^{-1}. The Raman spectra for the single crystals were analyzed with incident light of 633 nm wavelength when the orientations of the polarization vectors of the incident and scattered light were collinear with the longest morphological direction of a needle-like crystal.

3. Results and discussion

3.1. Structure analysis

In the crystal structure of (1), the interaction between the triiodide anion and a neighboring iodine-containing dihydrooxazinoquinolinium cation is achieved through an I1···I4*A* halogen bond of length 3.7386 (4) Å [Fig. 1; symmetry code: (*A*) $x+\frac{1}{2}, -y+\frac{3}{2}, z+\frac{1}{2}$]. The interaction is almost linear [C12—I1···I4*A* = 173.30 (6)°] between the σ-hole formed on extension of the C12—I1 covalent bond in the cation and the charge concentration area in the triiodide anion.

Our special attention is drawn to the relatively rare case of halogen bonding between the terminal atoms of neighbouring triiodide anions, *i.e.* $I_3^-\cdots I_3^-$. The length of the I2···I4*A* halogen bond between atoms belonging to similarly charged ions is 3.7171 (4) Å, which is shorter than the I1···I4*A* halogen bond, which is reinforced by opposite charges.

Note that zigzag-type chains of triiodide anions are not uncommon (Groenewald *et al.*, 2012) and most of them have an angle between the subunits which is closer to a straight angle (180°) than to a right angle (90°) (Miller, 2013). For example, the I_6^{2-} anion comprises two triiodide anions at an angle of 163.0°, and the distance between the terminal I atoms is 3.501 Å (van Megen & Reiss, 2013). The geometry of such a mutual orientation characterizes Type I contacts (Metrangolo & Resnati, 2014), which are not related to halogen bonds.

For the crystal structure of (1), we consider that the nature of the I2···I4*A* interaction as a typical halogen bond is beyond doubt. First, the main geometric criterion is satisfied, *i.e.* the I3—I2···I4*A* angle between neighbouring triiodide anions in a chain is 116.989 (11)°. Second, the area of charge concentration on the I2 atom is directed towards the σ-hole, which lies on the extension of the I3*A*—I4*A* bond of the triiodide anion.

We assume that the possibility of halogen bonding between a pair of triiodide anions, *i.e.* $I_3^-\cdots I_3^-$, is induced by a strong asymmetry of the bonds within the triiodide anion. Since the I2—I3 bond length is 3.0048 (2) Å and the I3—I4 bond length is 2.8708 (2) Å, the structure of this triiodide anion is close to the formal structure of a diiodine molecule bound to a monoiodide anion. Such a disproportion of the bond lengths in the triiodide anion explains the well-known electron-donating properties of the I2 atom and the fact that the I4 atom acts both as an electron donor in an I1···I4*A* halogen bond and as an electron acceptor in an I2···I4*A* halogen bond.

Note that despite the plausible participation of the Cl1 atom in halogen bonding, this is not observed in the crystal structure of salt (1).

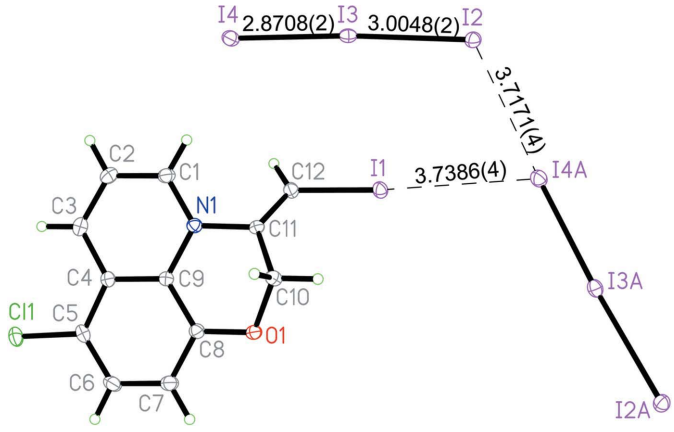

Figure 1
The cation and neighbouring anions connected by halogen bonds (dashed lines) in the crystal structure of salt (1). Displacement ellipsoids are drawn at the 50% probability level. [Symmetry code: (*A*) $x+\frac{1}{2}, -y+\frac{3}{2}, z+\frac{1}{2}$.]

The heterocyclic cations and triiodide anions form a layered packing (Fig. 2), in which a zigzag chain of triiodide anions is accompanied by ribbons of heterocyclic cations. This arrangement is mediated by the halogen bonds discussed above. Within the ribbon of cations, the mirror antipodes of the dihydrooxazinoquinolinium heterocycles alternate with each other. Their chirality is due to the planar asymmetry of the dihydrooxazinoquinolinium cyclic system.

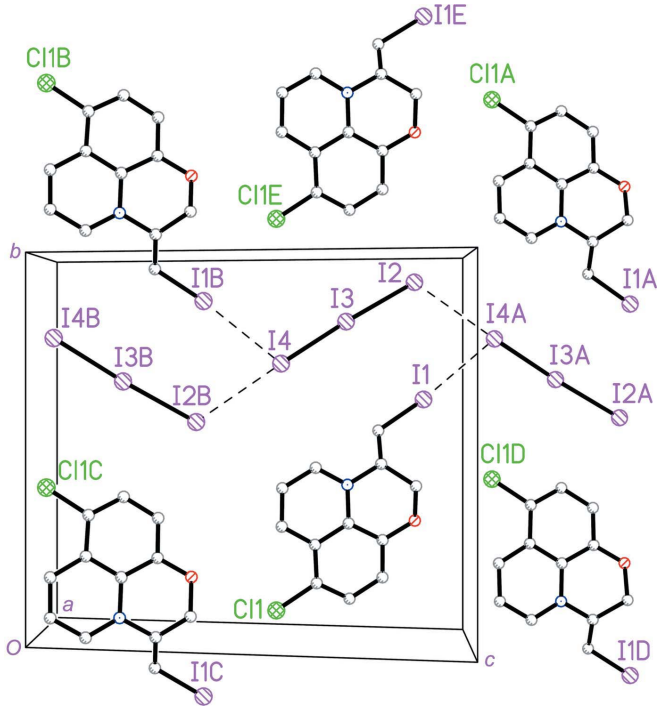

Figure 2
A fragment of the layered packing of (1), where the triiodide anions accompany a chain of heterocyclic cations. [Symmetry codes: (*A*) $x+\frac{1}{2}, -y+\frac{3}{2}, z+\frac{1}{2}$; (*B*) $x-\frac{1}{2}, -y+\frac{3}{2}, z-\frac{1}{2}$; (*C*) $x-\frac{1}{2}, -y+\frac{1}{2}, z-\frac{1}{2}$; (*D*) $x+\frac{1}{2}, -y+\frac{1}{2}, z+\frac{1}{2}$; (*E*) $x, y+1, z$.]

3.2. Raman spectra

The Raman spectrum of (1) obtained from the smooth brown single-crystal surface area shows an intense band at 149 cm^{-1} (Fig. 3). This band corresponds to the stretching vibration of the I3—I4 bond in the asymmetric triiodide anion. Such a situation is known for extremely asymmetric triiodides, *i.e.* $[I—I\cdots I]^-$ (Svensson &, Kloo, 2003; Deplano *et al.*, 1999; Ambrosetti *et al.*, 1991). In this case, only the band for bound molecular iodine ν(I—I) appears in the Raman spectrum, while the typical triiodide vibration bands, *i.e.* symmetric ν_{sym} (100–120 cm^{-1}) and asymmetric ν_{asym} (120–140 cm^{-1}) iodine–iodine vibrations, are not observed.

According to an empirical correlation between the observed wavenumbers and the interatomic I···I distances for the I3—I4 bond [2.8708 (2) Å], we can expect the vibration band to be in the range 145–150 cm^{-1} (Arca *et al.*, 2006). It is worth mentioning that the bond length in the title compound is close to the value suggested by Arca *et al.* (2006), *i.e.* ~2.86 Å, as a criterion for a the boundary between the two types of iodine adducts, namely weak adducts of the B···I—I type and medium–weak adducts of the B–I–I type, according to the classification of Deplano *et al.* (1999).

Some of the Raman spectra, obtained for different parts of the single-crystal surface under similar experimental conditions, show a band at 174 cm^{-1} of varying intensity. This band corresponds to the existence of a weakly bound diiodine molecule (Svensson &, Kloo, 2003; Deplano *et al.*, 1999; Yushina *et al.*, 2015). In the polarized spectrum of the single crystal of (I), only the band at 149 cm^{-1} is observed, while the band at 174 cm^{-1} is absent. The latter may thus be the result of triiodide decomposition and the further appearance of the weakly bound diiodine molecule on the surface of the crystal.

3.3. Thermal analysis

The presence of a bound diiodine molecule usually leads to an earlier start to the decomposition process in comparison with corresponding triiodides (van Megen & Reiss, 2013; Yushina *et al.*, 2011, 2013). Such a structural feature also causes the appearance of a separate peak for iodine loss without decomposition of the organic cation. In our case, we observed four stages of decomposition, according to the derivative thermogravimetric (DTG) curve: peak **I** corresponds to the loss of weakly bound molecular iodine, and peaks **II**, **III** and **IV** are similar to the previously observed data for nearly symmetric triiodides with a tricyclic chalcogenazinolo(ino)quinolinium cation. Peak **IV** corresponds to the oxidation of an organic cation and is highly exothermic according to the differential scanning calorimetry (DSC) curve.

The single crystal of (1) starts to decompose at a temperature close to the melting point of crystalline iodine; there is a 5% mass loss at 390 K. In the range 396–415 K, there is an endothermic peak on the DSC curve (Fig. 4) coinciding with the first decomposition stage (peak **I** on the DTG curve; Fig. 4). The temperature range of peak **I** is similar to the first

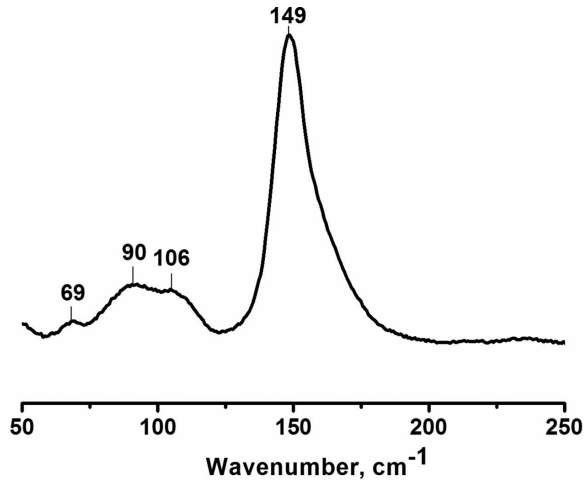

Figure 3
The low-frequency region of the Raman spectrum of salt (1).

stage of iodine loss for previously studied compounds exhibiting $I_3^-\cdots I_2$ halogen bonds (Yushina *et al.*, 2011, 2013). The mass loss for the crystal of salt (1) at the first stage of decomposition is 17%, which is twice lower than the expected value for the loss of a diiodine molecule. Thus, we can presume either the loss of I_2 from each triiodide anion or the loss of one I atom per anion. Comparison of our results with previously obtained data has revealed that after the loss of weakly bound iodine there is a stability plateau between peak **I** and peak **II** in (1) (Fig. 4), as distinct from polyiodides with an $I_3^-\cdots I_2$ structure. The observed features of thermal decomposition are in good agreement with the high asymmetry of the triiodide anion, *i.e.* $[I—I\cdots I]^-$. If we assume the loss of one I atom per anion, then the most weakly bound I atom is I2. Note that the band at 174 cm^{-1} in some Raman spectra corresponding to weakly bound iodine can be an argument in favour of this hypothesis.

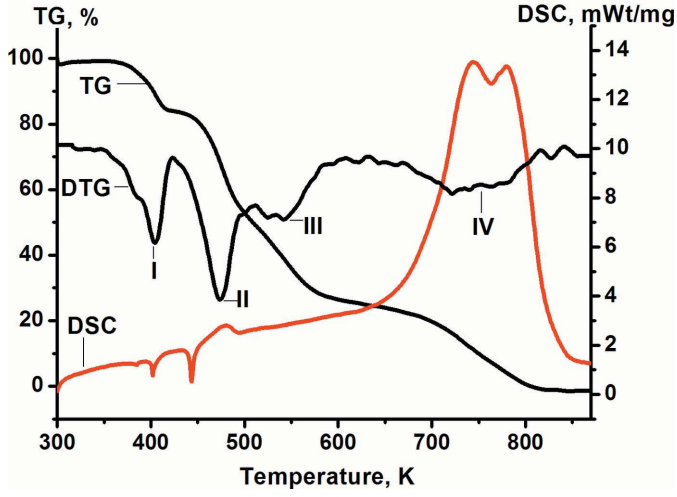

Figure 4
The thermal decomposition of salt (1) at a heating rate of 10 K min^{-1} in air.

4. Conclusion

Analysis of the crystal structure of a new triiodide, (1), reveals two kinds of iodine–iodine halogen bonds, namely between the I atom of the heterocyclic cation and the triiodide anion, which is typical for this class of compounds, and the extremely rare case of a halogen bond between the terminal atoms of neighbouring triiodide anions. Such nontypical halogen bonds are due to the strong disproportion of the iodine–iodine interactions in the triiodide anion.

A characteristic band at 149 cm^{-1} in the low-frequency region of the Raman spectrum of (I) definitely shows the existence of the asymmetric triiodide anion. Moreover, the spectra obtained for different regions of the crystal surface show vibrations attributed to weakly bound molecular iodine that can be the product of decomposition processes during sample storage.

An endothermic peak on the DSC curve in the range 396–415 K corresponds to the first stage of iodine loss from the crystalline state. The thermal decomposition features of (1) have much in common with polyiodides exhibiting $I_3^-\cdots I_2$ halogen bonds due to the high asymmetry of the iodine–iodine interactions in the triiodide anion. Raman spectroscopic data and thermal analysis have together revealed the properties caused by the existence of relatively weakly bound molecular iodine. These results essentially complement the X-ray diffraction data. Therefore, this study draws attention to chalcogenazinolo(ino)quinolinium triiodides as stable compounds susceptible to gradual iodine release from the crystal due to the unique partnering and combination of iodine–iodine halogen bonds in the considered crystal structure.

Acknowledgements

This work has been supported by the Ministry of Education and Science of the Russian Federation. We gratefully acknowledge the beam time obtained at the ChemMatCARS beam line at the Advanced Photon Source, Argonne National Laboratory. The synchrotron radiation XRD studies have been supported by the US Department of Energy, Office of Science (contract No. DEAC0206CH11357). ChemMatCARS Sector 15 is funded by the US National Science Foundation and US Department of Energy (project No. NSF/CHE0822838). We are grateful to Professor B. A. Kolesov, Nikolaev Institute of Inorganic Chemistry, Russian Academy of Sciences, Novosibirsk, for the opportunity to obtain Raman spectra.

References

Advanced Chemistry Development Inc. (2015). *ACD/ChemSketch*. Advanced Chemistry Development Inc., Toronto, ON, Canada. http://www.acdlabs.com.
Ambrosetti, R., Bellucci, G., Bianchini, R., Bigoli, F., Deplano, P., Pellinghelli, M. A. & Trogu, E. F. (1991). *J. Chem. Soc. Perkin Trans. 2*, pp. 339–347.
Arca, M., Aragoni, M. C., Devillanova, F. A., Garau, A., Isaia, F., Lippolis, V., Mancini, A. & Verani, G. (2006). *Bioinorg. Chem. Appl.* pp. 58937–58949.
Bartashevich, E. V., Nasibullina, S. E., Bol'shakov, O. I. & Tsirelson, V. G. (2015). *Struct. Chem.* **12**, 1–9.
Bartashevich, E. V., Yushina, I. D., Stash, A. I. & Tsirelson, V. G. (2014). *Cryst. Growth Des.* **14**, 5674–5684.
Bruker (2013). *SAINT*, *SADABS*, *APEX2* and *SHELXTL*. Bruker AXS Inc., Madison, Wisconsin, USA
Deplano, P., Ferraro, J. R., Mercuri, M. L. & Trogu, E. F. (1999). *Coord. Chem. Rev.* **188**, 71–95.
Desiraju, G. R., Ho, P. S., Kloo, L., Legon, A. C., Marquardt, R., Metrangolo, P., Politzer, P. A., Resnati, G. & Rissanen, K. (2013). *Pure Appl. Chem.* **85**, 1711–1713.
Gilday, L. C., Robinson, S. W., Barendt, T. A., Langton, M. J., Mullaney, B. R. & Beer, P. D. (2015). *Chem. Rev.* **115**, 7118–7195.
Groenewald, F., Esterhuysen, C. & Dillen, J. (2012). *Theor. Chem. Acc.* **131**, article 1281.
Kim, D. G. (2008). *Khim. Geterotsikl. Soedin.* **11**, 1664–1668.
Megen, M. van & Reiss, G. J. (2013). *Inorganics*, **1**, 3–13.
Metrangolo, P., Meyer, F., Pilati, T., Resnati, G. & Terraneo, G. (2008). *Angew. Chem. Int. Ed.* **47**, 6114–6127.
Metrangolo, P. & Resnati, G. (2014). *IUCrJ*, **1**, 5–7.
Miller, J. (2013). In *Extended Linear Chain Compounds*. Berlin: Springer Science & Business Media.
Punyani, S., Narayana, P., Singh, H. & Vasudevan, P. (2006). *J. Sci. Ind. Res.* **65**, 116–120.
Sheldrick, G. M. (2008). *Acta Cryst.* A**64**, 112–122.
Sheldrick, G. M. (2015). *Acta Cryst.* C**71**, 3–8.
Svensson, P. H. & Kloo, L. (2003). *Chem. Rev.* **103**, 1649–1684.
Yushina, I., Bartashevich, E., Zherebtsov, D., Kim, D. & Batalov, V. (2011). Proceedings of the 1st Central and Eastern European Conference on Thermal Analysis and Calorimetry (CEEC–TAC), Craiova, Romania, 7–10 September 2011. Abstracts, p. 388.
Yushina, I., Batalov, V., Kim, D. & Bartashevich, E. (2013). Proceedings of the 2nd Central and Eastern European Conference on Thermal Analysis and Calorimetry (CEEC–TAC2), Vilnius, Lithuania, 27–30 August 2013. Abstracts, OP1.11, p. 85.
Yushina, I., Kolesov, B. & Bartashevich, E. (2015). *New J. Chem.* **39**, 6163–6170.

supporting information

Acta Cryst. (2016). C**72**, 341-345 [doi:10.1107/S2053229616003934]

Nontypical iodine–halogen bonds in the crystal structure of (3*E*)-8-chloro-3-iodomethylidene-2,3-dihydro-1,4-oxazino[2,3,4-*ij*]quinolin-4-ium triiodide

E. V. Bartashevich, V. I. Batalov, I. D. Yushina, A. I. Stash and Y. S. Chen

Computing details

Data collection: *APEX2* (Bruker, 2013); cell refinement: *SAINT* (Bruker, 2013); data reduction: *SAINT* (Bruker, 2013); program(s) used to solve structure: *SHELXS97* (Sheldrick, 2008); program(s) used to refine structure: *SHELXL2013* (Sheldrick, 2015); molecular graphics: *SHELXTL* (Bruker, 2013) and *ACD/ChemSketch* (Advanced Chemistry Development Inc., 2015); software used to prepare material for publication: *SHELXTL* (Bruker, 2013).

(3*E*)-8-Chloro-3-iodomethylidene-2,3-dihydro-1,4-oxazino[2,3,4-*ij*]quinolin-4-ium triiodide

Crystal data

$C_{12}H_8ClINO^+\cdot I_3^-$
M_r = 725.24
Monoclinic, $P2_1/n$
a = 7.6227 (2) Å
b = 13.9464 (4) Å
c = 16.0161 (4) Å
β = 101.6439 (7)°
V = 1667.62 (8) Å^3
Z = 4
$F(000)$ = 1296
D_x = 2.889 Mg m^{-3}
Synchrotron radiation, λ = 0.41328 Å
Cell parameters from 9796 reflections
θ = 2.3–17.2°
μ = 1.75 mm^{-1}
T = 100 K
Prism, brown
0.04 × 0.03 × 0.01 mm

Data collection

Bruker APEXII CCD diffractometer
Radiation source: Advanced photon source
Diamond (111) monochromator
φ–scan
Absorption correction: multi-scan (*SADABS*; Bruker, 2013)
T_{min} = 0.842, T_{max} = 0.955
45635 measured reflections
5066 independent reflections
4500 reflections with $I > 2\sigma(I)$
R_{int} = 0.048
θ_{max} = 17.2°, θ_{min} = 1.5°
h = −10→10
k = −19→19
l = −22→20

Refinement

Refinement on F^2
Least-squares matrix: full
$R[F^2 > 2\sigma(F^2)]$ = 0.016
$wR(F^2)$ = 0.035
S = 1.04
5066 reflections
172 parameters
0 restraints
Primary atom site location: difference Fourier map
Secondary atom site location: difference Fourier map
Hydrogen site location: inferred from neighbouring sites
H-atom parameters constrained
$w = 1/[\sigma^2(F_o^2) + (0.0066P)^2 + 1.3647P]$ where $P = (F_o^2 + 2F_c^2)/3$
$(\Delta/\sigma)_{max}$ = 0.002
$\Delta\rho_{max}$ = 0.59 e Å^{-3}
$\Delta\rho_{min}$ = −0.52 e Å^{-3}

Special details

Experimental. The crystal was cooled to 100 (2) K using the Cryojet N2 cold stream. The data collection was performed in φ-scan mode using steps of 0.5° and with fixed ω and χ angles.

Geometry. All e.s.d.'s (except the e.s.d. in the dihedral angle between two l.s. planes) are estimated using the full covariance matrix. The cell e.s.d.'s are taken into account individually in the estimation of e.s.d.'s in distances, angles and torsion angles; correlations between e.s.d.'s in cell parameters are only used when they are defined by crystal symmetry. An approximate (isotropic) treatment of cell e.s.d.'s is used for estimating e.s.d.'s involving l.s. planes.

Fractional atomic coordinates and isotropic or equivalent isotropic displacement parameters (Å²)

	x	*y*	*z*	U_{iso}*/U_{eq}
I1	0.66498 (2)	0.62361 (2)	0.89967 (2)	0.01440 (3)
I2	0.73791 (2)	0.93112 (2)	0.88024 (2)	0.01641 (3)
I3	0.56775 (2)	0.82664 (2)	0.72026 (2)	0.01462 (3)
I4	0.41517 (2)	0.71760 (2)	0.57124 (2)	0.01730 (4)
Cl1	0.31958 (7)	0.08762 (4)	0.56172 (3)	0.01759 (10)
O1	0.5294 (2)	0.31342 (10)	0.87713 (9)	0.0146 (3)
N1	0.3789 (2)	0.40884 (12)	0.72295 (11)	0.0122 (3)
C1	0.2998 (3)	0.45397 (14)	0.65133 (13)	0.0151 (4)
H1	0.2873	0.5217	0.6516	0.018*
C2	0.2358 (3)	0.40311 (15)	0.57665 (14)	0.0166 (4)
H2	0.1778	0.4360	0.5267	0.020*
C3	0.2567 (3)	0.30512 (15)	0.57515 (14)	0.0153 (4)
H3	0.2150	0.2705	0.5239	0.018*
C4	0.3397 (3)	0.25623 (14)	0.64956 (13)	0.0117 (4)
C5	0.3740 (3)	0.15615 (14)	0.65342 (13)	0.0138 (4)
C6	0.4558 (3)	0.11316 (14)	0.72781 (14)	0.0172 (4)
H6	0.4793	0.0462	0.7286	0.021*
C7	0.5055 (3)	0.16687 (14)	0.80322 (14)	0.0166 (4)
H7	0.5597	0.1356	0.8547	0.020*
C8	0.4766 (3)	0.26435 (14)	0.80322 (13)	0.0129 (4)
C9	0.3973 (3)	0.30951 (14)	0.72569 (12)	0.0110 (3)
C10	0.4431 (3)	0.40542 (14)	0.87812 (13)	0.0140 (4)
H101	0.5007	0.4417	0.9295	0.017*
H102	0.3154	0.3961	0.8803	0.017*
C11	0.4574 (3)	0.46079 (14)	0.79981 (13)	0.0122 (4)
C12	0.5393 (3)	0.54442 (14)	0.79424 (13)	0.0137 (4)
H12	0.5404	0.5692	0.7391	0.016*

Atomic displacement parameters (Å²)

	U^{11}	U^{22}	U^{33}	U^{12}	U^{13}	U^{23}
I1	0.01625 (7)	0.01324 (6)	0.01395 (6)	−0.00313 (5)	0.00358 (5)	−0.00033 (5)
I2	0.01699 (7)	0.01690 (6)	0.01509 (7)	0.00253 (5)	0.00264 (5)	−0.00017 (5)
I3	0.01396 (6)	0.01403 (6)	0.01650 (7)	0.00317 (5)	0.00456 (5)	0.00226 (5)
I4	0.02154 (7)	0.01424 (6)	0.01651 (7)	0.00171 (5)	0.00477 (6)	0.00024 (5)
Cl1	0.0181 (2)	0.0159 (2)	0.0182 (2)	−0.00220 (18)	0.00227 (19)	−0.00602 (18)
O1	0.0193 (7)	0.0118 (6)	0.0118 (7)	0.0022 (5)	0.0013 (6)	0.0010 (5)

N1	0.0136 (8)	0.0117 (7)	0.0114 (8)	−0.0001 (6)	0.0033 (6)	0.0008 (6)
C1	0.0169 (9)	0.0137 (8)	0.0145 (9)	0.0020 (7)	0.0024 (8)	0.0026 (7)
C2	0.0173 (10)	0.0192 (9)	0.0128 (9)	0.0016 (8)	0.0017 (8)	0.0022 (8)
C3	0.0133 (9)	0.0192 (9)	0.0135 (9)	−0.0011 (8)	0.0025 (8)	−0.0016 (8)
C4	0.0089 (8)	0.0133 (8)	0.0135 (9)	−0.0014 (7)	0.0034 (7)	−0.0002 (7)
C5	0.0131 (9)	0.0129 (8)	0.0163 (9)	−0.0023 (7)	0.0050 (8)	−0.0036 (7)
C6	0.0189 (10)	0.0110 (8)	0.0218 (11)	−0.0008 (7)	0.0040 (9)	0.0012 (8)
C7	0.0191 (10)	0.0142 (9)	0.0161 (10)	0.0014 (8)	0.0030 (8)	0.0030 (7)
C8	0.0123 (8)	0.0126 (8)	0.0137 (9)	−0.0008 (7)	0.0023 (7)	0.0010 (7)
C9	0.0102 (8)	0.0114 (8)	0.0119 (9)	0.0007 (7)	0.0033 (7)	0.0003 (7)
C10	0.0158 (9)	0.0116 (8)	0.0148 (9)	0.0001 (7)	0.0040 (8)	0.0000 (7)
C11	0.0135 (9)	0.0117 (8)	0.0112 (8)	0.0007 (7)	0.0018 (7)	0.0020 (7)
C12	0.0151 (9)	0.0128 (8)	0.0133 (9)	−0.0009 (7)	0.0032 (8)	−0.0010 (7)

Geometric parameters (Å, º)

I1—C12	2.082 (2)	C3—H3	0.9500
I2—I3	3.0048 (2)	C4—C5	1.419 (3)
I3—I4	2.8708 (2)	C4—C9	1.420 (3)
Cl1—C5	1.731 (2)	C5—C6	1.367 (3)
O1—C8	1.356 (2)	C6—C7	1.407 (3)
O1—C10	1.443 (2)	C6—H6	0.9500
N1—C1	1.340 (3)	C7—C8	1.377 (3)
N1—C9	1.392 (2)	C7—H7	0.9500
N1—C11	1.450 (3)	C8—C9	1.414 (3)
C1—C2	1.391 (3)	C10—C11	1.496 (3)
C1—H1	0.9500	C10—H101	0.9900
C2—C3	1.377 (3)	C10—H102	0.9900
C2—H2	0.9500	C11—C12	1.334 (3)
C3—C4	1.408 (3)	C12—H12	0.9500
I4—I3—I2	176.897 (6)	C7—C6—H6	119.6
C8—O1—C10	113.73 (15)	C8—C7—C6	120.67 (19)
C1—N1—C9	121.30 (17)	C8—C7—H7	119.7
C1—N1—C11	121.96 (17)	C6—C7—H7	119.7
C9—N1—C11	116.66 (16)	O1—C8—C7	118.60 (18)
N1—C1—C2	121.02 (19)	O1—C8—C9	122.72 (17)
N1—C1—H1	119.5	C7—C8—C9	118.66 (19)
C2—C1—H1	119.5	N1—C9—C8	119.55 (17)
C3—C2—C1	119.96 (19)	N1—C9—C4	118.81 (17)
C3—C2—H2	120.0	C8—C9—C4	121.62 (18)
C1—C2—H2	120.0	O1—C10—C11	109.83 (17)
C2—C3—C4	119.99 (19)	O1—C10—H101	109.7
C2—C3—H3	120.0	C11—C10—H101	109.7
C4—C3—H3	120.0	O1—C10—H102	109.7
C3—C4—C5	124.10 (19)	C11—C10—H102	109.7
C3—C4—C9	118.81 (18)	H101—C10—H102	108.2
C5—C4—C9	117.08 (18)	C12—C11—N1	119.93 (18)

C6—C5—C4	121.13 (19)	C12—C11—C10	128.45 (19)
C6—C5—Cl1	119.11 (16)	N1—C11—C10	111.49 (16)
C4—C5—Cl1	119.72 (16)	C11—C12—I1	123.66 (16)
C5—C6—C7	120.76 (19)	C11—C12—H12	118.2
C5—C6—H6	119.6	I1—C12—H12	118.2